AALBORG UNIVERSITY

DENMARK

Multi-Functional Distributed Generation Unit for Power Quality Enhancement

Zeng, Zheng; Yang, Huan; Guerrero, Josep M.; Zhao, Rongxiang

A Multi-Functional Distributed Generation Unit for Power Quality Enhancement

Zheng Zeng[a], Huan Yang[b], Josep M. Guerrero[c], and Rongxiang Zhao[b]

a. State Key Laboratory of Power Transmission Equipment & System Security and New Technology, College of Electrical Engineering, Chongqing University, Chongqing 400044, China

b. College of Electrical Engineering, Zhejiang University, Hangzhou 310027, Zhejiang Province, China

c. Department of Energy Technology, Aalborg University, Aalborg DK 9220, Denmark

Abstract—A multi-functional distributed generation unit (MFDGU) and its control strategy are proposed in this paper for the purpose of enhancing power quality in low-voltage networks. By using the 3H-bridge converter structure, an MFDGU can be applied in 3-phase 4-wire low-voltage distribution networks to compensate harmonic, reactive, and unbalanced currents. A reduced-order model of the MFDGU is derived through a weighted-average-current-feedback (WACF) approach, showing the robustness and stability of the proposed approach. The Fryze-Buchholz-Dpenbrock (FBD) power theory is employed to generate the current reference of the MFDGU, which can be easily implemented in three-phase networks. A 15kVA prototype consisting of three full bridge converters has been built and tested. Experimental results show the feasibility of the proposed topology and control strategy.

Index Terms—3H-bridge converter, distributed generation, multi-functional grid-connected inverter, power quality enhancement

Nomenclature

i_{1abc}	Inductor current of the LC filter
i_{2abc}	Output current of the multi-functional distributed generation unit (MFDGU)
i_{gabc}	Utility-side current of the MFDGU module
i_{Labc}	Load-side current of the MFDGU module (or the equivalent downstream load current of the MFDGU)
u_{gabc}	Voltage in MFDGU terminals
u_{oabc}	MFDGU legs average output voltage
L, C, R	Inductor, capacitor, and damping resistor of the LC filter
L_1, L_2	Primary and secondary leakage inductors of the isolation transformer
L_g	Equivalent inductor of the utility grid impedance
R_{uabc}, C_u	Resistors and capacitor of the unbalance load
R_r	Nonlinear diode-rectifier load resistor

1 Introduction

With the increasing penetration of distributed renewable energy sources (RESs) embedded into the utility grid, power quality of distributed generation systems (DGSs) has become an important issue [1-3]. Topologies and control strategies of grid-connected converter have been extensively investigated, as components to connect RESs into the utility grids [4-8]. In a DGS, reactive, harmonic, and unbalanced current generated by local loads may not only degrade the power quality at the point of common coupling (PCC), but also may result in instabilities due to series and/or parallel harmonic resonances [9-10].

Two typical strategies are usually used to address these issues. One focuses on using advanced control strategies to improve the output current waveforms and to enhance uninterruptable operation capability of grid-connected converters in abnormal utility

conditions [11-13]. Nevertheless, this strategy may not be able to definitely suppress the already poor power quality contribution of DGSs. The other strategy solves the power quality problem by employing some dedicated power quality conditioners, such as active power filters (APF), dynamic voltage regulators (DVR), static synchronous compensators (STATCOM), and unified power quality conditioners (UPQC) [14-17]. This strategy is much more popular due to its flexibility. However, either a passive or an active conditioner needs an additional device to be installed. Hence, there are inevitable drawbacks, such as increased cost, power rating, size, and man-hour.

Some grid-connected power converters incorporate additional functionalities, such as reactive power compensation, harmonics elimination, and unbalanced power correction, and can provide useful auxiliary services to enhance the power quality from the viewpoint of DGSs [10, 18-23]. In other words, as a high-level approach to integrate RESs, DGSs based on power electronics are able to play an important role in low-voltage (LV) distribution networks by providing ancillary services to the utility grid. Such ancillary services depend on the capabilities of these grid-connected converters [4]. It is suggested that power converters in DGSs should follow references from hierarchical control structures, where each power converter should operate in either grid-feeding or grid-supporting mode [4, 24]. The multi-functional distributed generation unit (MFDGU) is regarded as an attractive approach, which not only improves the power quality performance of DGSs, but also upgrades the DGSs themselves [25-26].

For LV distribution systems, 3-phase 4-wire (3p4w) is the most common configuration, in which line current distortion, non-unity power factor, and unbalanced 3 phase voltages are the typical power quality issues. Consequently, some MFDGU topologies have been proposed in the literature for 3p4w LV distribution networks. Due to the superiority in compensating the unbalance power, converters based on single-phase H-bridge [27] and

3-phase 4-leg topologies [28] have been received much attention. Furthermore, the 3H-bridge converter is also a good choice for 3p4w due to its modular topology and low voltage stress. In [29], a distributed generation unit (DGU) equipped with 3H-bridge is introduced for micro-grid power quality enhancement and load sharing capability. To coordinate with other DGUs in a micro-grid, one-way broadcasting communication is utilized in [30]. Simulation results are used to verify its effectiveness, but no experimental test has been carried out. In addition, the need of a communication channel for DGU coordination is an important drawback of the proposed control. If communication fails, the whole micro-grid may be shut down. As indicated in [31-32], modular coordinated MFDGU schemes without relying on a single communication channel should be further studied.

This paper reports an in-depth investigation and experimental validation of a modular MFDGU topology based on a 3H-bridge converter and its control strategy. The rest of the paper is organized as follows. Section 2 outlines the MFDGU configuration and develops its reduced-order dynamical model by using the weighted-average-current-feedback (WACF) control strategy. In Section 3, the experimental setup of a 15kVA prototype is briefly described, and the experimental results are presented and critically analyzed. Section 4 extends a discussion on the applications of MFDGU. Finally, Section 5 concludes this paper.

2 Mathematical model and control strategy of the MFDGU

2.1 Reduced-order modelling approach

The configuration of the MFDGU topology studied in this paper is shown in Fig. 1(a). The basic MFDGU topology consists of a single-phase H-bridge converter and an LC filter. Therefore, in a 3p4w LV distribution network, the whole three-phase system can be regarded as three independent single-phase systems. Consequently, it is easy to enhance the power quality via a modular design, especially for power unbalance compensation. Additionally, the MFDGU module can be in parallel with the feeder of a DGS like the conventional grid-connected inverter. However, beside the output current i_{1abc} and i_{2abc}, the MFDGU also

feeds back the current i_{Labc} and views it as the equivalent current of downstream loads. Power quality issues, such as reactive, harmonic, and unbalanced current, can be compensated by the MFDGU by using the control scheme presented in the following subsections. Note that when MFDGUs are applied in 3p4w LV distribution networks, isolation transformers are required to work together with the LC filters. Apart from galvanic isolation and step-up functions, isolation transformers associated with LC filters may form the inverter output impedance that reduces the electrical impact of the MFDGU in the utility. Three single-phase H-bridges constitute phases *a*, *b*, and *c*, respectively, and LC filters are used as links between inverters and isolation transformers. Secondary sides of the transformers are connected to the distribution network, in which there may be nonlinear, reactive, and unbalanced loads.
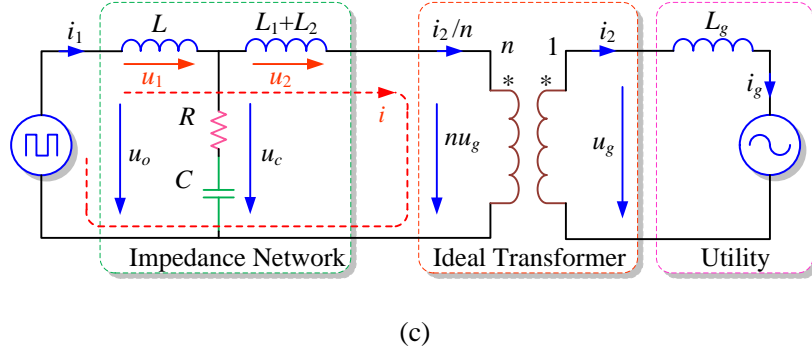

(a)

(b)

(c)
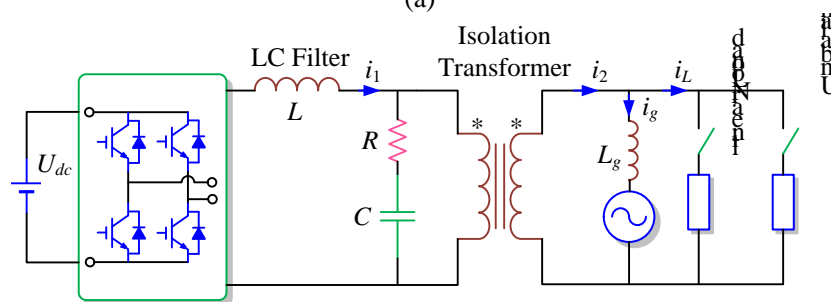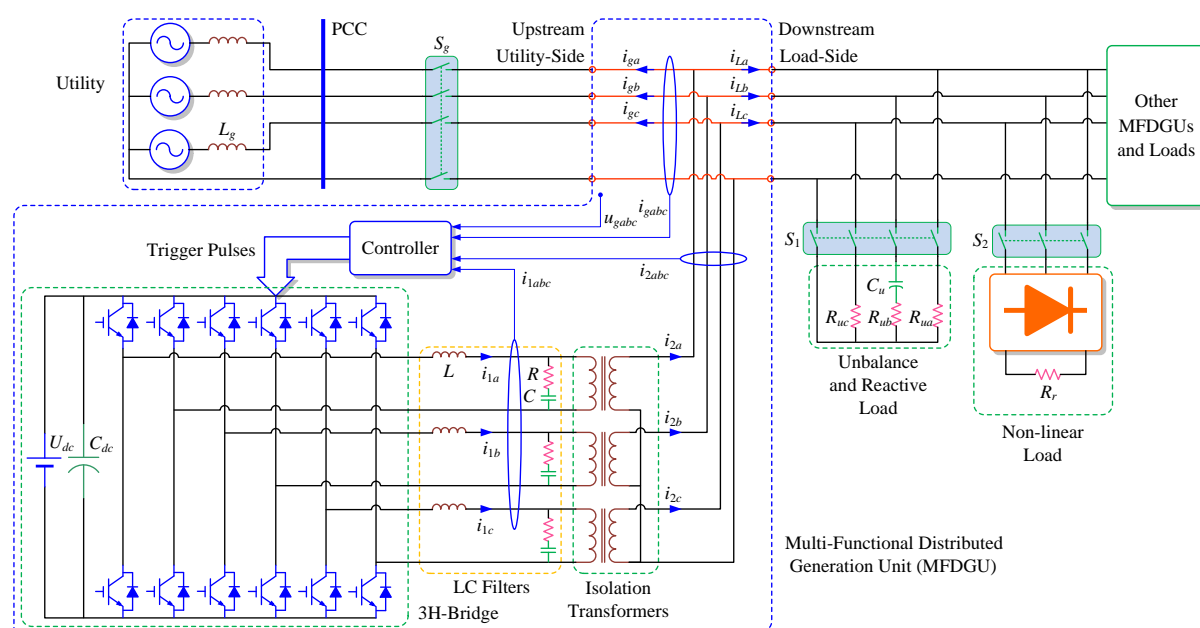
Fig. 1. Configuration of MFDGU. (a) A DGS includes MFDGU, (b) schematic circuit of the single-phase MFDGU, and (c) detailed equivalent circuit model of the single-phase MFDGU topology.

As shown in Fig. 1(a), the utility is neutral-connected, so that the 3-phase system can be regarded as three single-phase systems. As a result, the three single-phase H-bridges are decoupled from each other, and they can act as three independent single-phase grid-connected converters, as illustrated in Fig. 1(b). To analyze the detailed model of the MFDGU topology, the effect of loads is neglected. In this study, it is assumed that the parameters of each phase are the same. Thus, the detailed equivalent circuit in Fig. 1(b) can be demonstrated as Fig. 1(c) shown, where L_1 and L_2 are the primary and secondary leakage inductances of the isolation transformer. Note that the magnetizing inductance L_m value is large that can be neglected in Fig. 1(c). L_m and L_2 are referred to the primary side; L, C, and R are the inductance, capacitance, and damping resistance of the LC filter, respectively; L_g is the internal inductance of the utility; u_o and u_g denote the output average voltage of the converter and the utility voltage, respectively; $n = N_1 : N_2$ denotes the turns ratio of the transformer windings; i_1 and i_2 are the filter inductor current and the MFDGU output current , respectively.

According to Fig. 1(c), if the parameters of three phases are balanced, a detailed dynamical

6

model of the MFDGU can be developed by using transfer functions. Taking an arbitrary phase, to avoid the complexity in modelling, the damping resistance R of the LC filter is so small that can be neglected in the modelling process.

As depicted in Fig. 1(c), the transfer function from u_o to i_2 is

$$G_{u_o \to i_2} = n \frac{1}{L(L_1 + L_2)Cs^3 + (L + L_1 + L_2)s} \tag{1}$$

Similarly, the transfer function from u_o to i_1 can be expressed as

$$G_{u_o \to i_1} = \frac{(L_1 + L_2)Cs^2 + 1}{L(L_1 + L_2)Cs^3 + (L + L_1 + L_2)s} \tag{2}$$

The transfer functions, from u_g to i_1, and from u_g to i_2, can be, respectively, written as

$$G_{u_g \to i_2} = -\frac{n^2(LCs^2 + 1)}{L(L_1 + L_2)Cs^3 + (L + L_1 + L_2)s} \tag{3}$$

$$G_{u_g \to i_1} = -\frac{n}{L(L_1 + L_2 + C)s^3 + (L + L_1 + L_2)s} \tag{4}$$

As a result, the block diagram of the MFDGU can be simplified as shown in Fig. 2(a). Note that i_{ref} is the reference current, $K_{pwm} = U_{dc}$ is the gain of the converter, and the PI controller takes the form $\text{PI} = K_p + K_i/s$, where K_p and K_i are the proportional and integral gains, respectively. If the output line-current i_2 is feed-back for control, as shown in Fig. 2(a), the close-loop of the model can be expressed as

$$I_2(s) = \frac{1}{1 + PI \times K_{pwm}G_{u_o \to i_2}} I_{ref}(s) + \frac{1}{1 + PI \times K_{pwm}G_{u_o \to i_2}} U_g(s) \tag{5}$$

where I_{ref} is the current reference of the MFDGU. Thus, the characteristic equation of (5) can be derived as

$$\Delta = L(L_1 + L_2)Cs^4 + (L + L_1 + L_2)s^2 + K_p K_{pwm}s + K_i K_{pwm} \tag{6}$$

Since there is no s^3 term in (6), according to Routh-Hurwitz stability criterion, the close-loop model is unstable. In this case, by introducing an extra s^3 term, some active or passive

7

damping methods may be effective to enhance the stability of the close-loop model as indicated in [33]-[34]. On the contrary, if the converter-side current i_1 is the feed-back to the controller, the close-loop model can be rewritten as

$$I_1(s) = \frac{1}{1 + PI \times K_{pwm} G_{u_o \to i_1}} I_{ref}(s) + \frac{1}{1 + PI \times K_{pwm} G_{u_o \to i_1}} U_g(s) \tag{7}$$

Similarly, the characteristic equation of (7) can be derived as

$$\Delta = L(L_1 + L_2)Cs^4 + (L_1 + L_2)CK_p K_{pwm}s^3$$
$$+ \left[(L + L_1 + L_2) + (L_1 + L_2)CK_i K_{pwm} \right]s^2 + K_p K_{pwm}s + K_i K_{pwm} \tag{8}$$

It can be seen from (8) that, the close-loop system may be stable if the PI gains are well designed to meet the Routh-Hurwitz stability criterion. However, as indicated in [33], although the system is stable with i_1 as feed-back, the bandwidth of the PI controller and the switching frequency are strictly limited due to resonance of the LCL structure. Therefore, some advanced feed-back controls with multiple currents should be introduced.

(a)

(b)

8
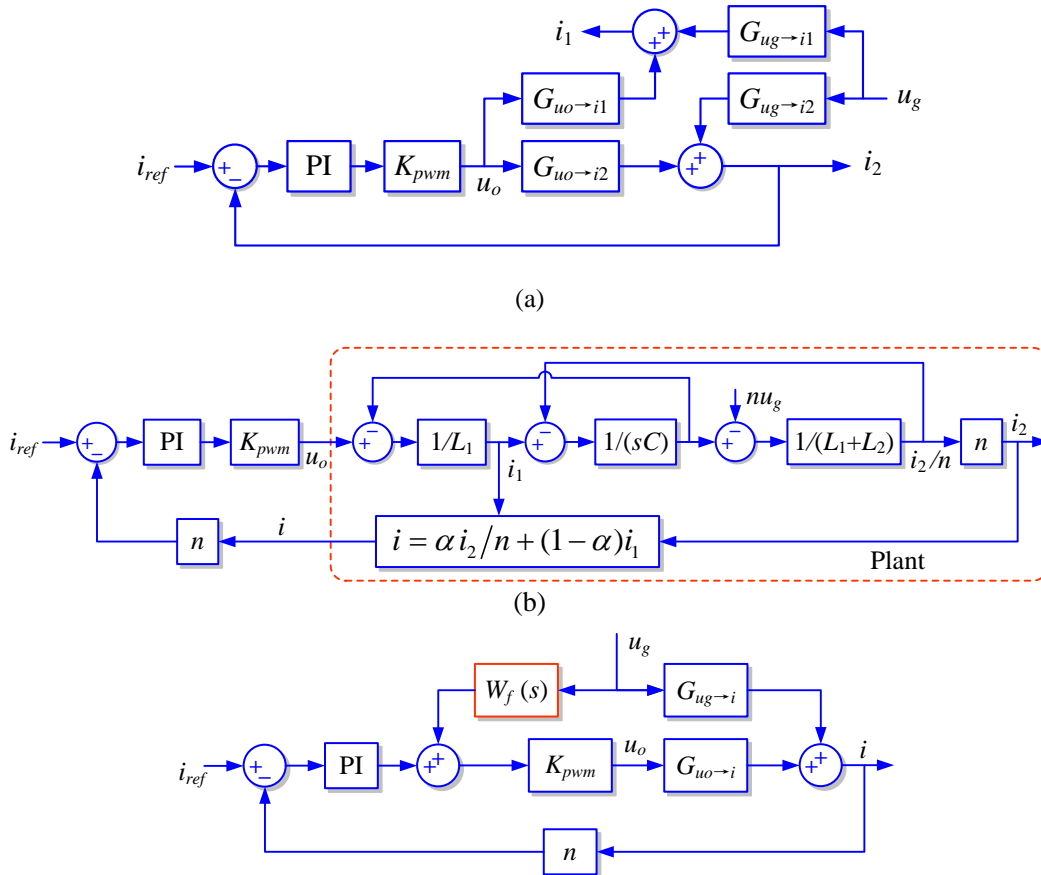
(c)

Fig. 2. Block diagrams of the closed-loop MFDGU. (a) Original model of the MFDGU, (b) reduced-order model of the MFDGU using WACF, and (c) model of the MFDGU with a PI and a feed-forward controllers.

In [35], a novel WACF control strategy has been presented, which can effectively reduce the third-order model of a grid-connected converter with LCL filter to a first-order one. This idea is implemented to reduce the full model of the MFDGU. The weighted-average-current or the equivalent virtual current of the MFDGU for feedback control purposes is defined as

$$i = \alpha i_2 / n + (1-\alpha) i_1 \tag{9}$$

where α is a weight coefficient. Then, the transfer function from u_o to i can be derived as follows

$$G_{u_o \to i} = \frac{\alpha}{n} G_{u_o \to i_2} + (1-\alpha) G_{u_o \to i_1} = \frac{(1-\alpha)(L_1 + L_2)Cs^2 + 1}{(L_1 + L_2 + L)s \left[\frac{(L_1 + L_2)LC}{L_1 + L_2 + L} s^2 + 1 \right]} \tag{10}$$

As can be found in (10), two poles can be cancelled by the zeroes, if the weight coefficient α is chosen as

$$\alpha = (L_1 + L_2) / (L + L_1 + L_2) \tag{11}$$

According to (11), (10) can then be simplified as

$$G_{u_o \to i} = \frac{1}{(L + L_1 + L_2)s} \tag{12}$$

Similarly, according to (3) and (4), the transfer function from u_g to i also can be derived as

$$G_{u_g \to i} = \frac{\alpha}{n} G_{u_g \to i_2} + (1-\alpha) G_{u_g \to i_1} = -n \frac{\alpha LCs^2 + 1}{(L_1 + L_2 + L)s \left[\frac{L(L_1 + L_2)C}{L_1 + L_2 + L} s^2 + 1 \right]} \tag{13}$$

If the coefficient α is chosen as the one shown in (11), (13) can be simplified as

9

$$G_{u_g \to i} = -\frac{n}{(L + L_1 + L_2)s} \tag{14}$$

The reduced-order models are the ones as defined in (12) and (14), which indicate that the system models mainly depend on the inductance value. Furthermore, the simplified model is a first-order system, which ensures that the PI controller can be easily designed. On the contrary, the original model before order-reduction is indicated in (1) and (3) (transfer functions $G_{u_o \to i_2}$ and $G_{u_g \to i_2}$). Here, the original model is a third-order one due to the three energy storage elements in Fig. 1(c). According to the poles of (1) and (3), the resonant frequency f_{res} of the model is

$$f_{res} = \frac{1}{2\pi} \sqrt{\frac{L + L_1 + L_2}{L(L_1 + L_2)C}} \tag{15}$$

The key parameters of the detailed MFDGU in Fig. 1(c) are listed in Tab. 1. Substituting these into (15), it is found that f_{res} = 2.25kHz. Fig. 3 illustrates the Bode diagram of the original and reduced-order models. It can be observed that reduced-order models are well approximated to the full-order models well when frequency f is lower than f_{res}, while there is clear deviation around and above f_{res}. The robustness of reduced-order models to immunize the parameter variation of inductors is also verified in Fig. 3. When using WACF control, the inductance deviates from its nominal value, resonance around f_{res} will occur again due to the pole-zero cancellation inaccuracy, as shown in Fig. 3.

Owing to the reduced-order model based on the WACF control, the LCL filter in Fig. 1(c), which includes the LC filter and the isolation transformer, can be considered as an equivalent L filter. According to [33] an LCL filter can be approximated an L filter when the operational frequency of concern is lower than the resonant frequency f_{res}. Nevertheless, this approximation is not valid for high-frequency harmonics and the LCL filter resonance frequency. Nevertheless, in a clear contribution of [33], by using the virtual current in (9), the

LCL filter can be well approximated to an L filter in the whole frequency domain. As shown in Fig. 1(c), based on the defined virtual current i, the total inductor voltage of the filter can be expressed as

$$
\begin{aligned}
U(s) &= U_1(s) + U_2(s) = I_1(s)sL + \frac{1}{n}I_2(s)s(L_1 + L_2) \\
&= U_o(s) - U_g(s) = I(s)(L + L_1 + L_2)s
\end{aligned}
\tag{16}
$$

where $L_1 + L_2$ is the leakage inductors. Thus,

$$
\begin{aligned}
I(s) &= I_1(s)\frac{sL}{(L + L_1 + L_2)s} + \frac{1}{n}I_2(s)\frac{s(L_1 + L_2)}{(L + L_1 + L_2)s} \\
&= I_1(s)\frac{L}{L + L_1 + L_2} + \frac{1}{n}I_2(s)\frac{L_1 + L_2}{L + L_1 + L_2} \\
&= (\alpha/n)I_2(s) + (1 - \alpha)I_1(s)
\end{aligned}
\tag{17}
$$

Consequently, comparing (9) and (17) shows that, from the point of view of the virtual current i, the LCL filter can be equivalent to an L filter. However, from the point of view of the current i_1 or i_2, the simplification of LCL filter as an L filter is not correct in any part of the frequency domain as pointed out in [33]. Although the resonance of the LCL filter is hidden in the WACF control as shown in (12) and (14), due to the pole-zero cancellation in practice, the resonance still remains. As a result, the WACF approach is not an active damping method, but a tool to analyze the stability and to simplify the control of the MFDGU. Therefore, an additional damping resistor R is employed to suppress possible resonances in the filter due to the pole-zero cancellation inaccuracy.

Tab. 1. Key parameters of the experimental MFDGU test bed.

Elements	Parameters and values
DC source	Voltage $U_{dc} = 400\text{V}$
	DC Capacitor $C_{dc} = 4400\mu\text{F}$
LC filter	Inductor $L = 1\text{mH}$
	Capacitor $C = 10\mu\text{F}$
	Damping resistor $R = 4\Omega$

| Isolation transformer	Winding turns ratio $n = N_1 : N_2 = 150 : 220$
	Primary and secondary leakage inductor $L_1 = L_2 = 0.5\text{mH}$
	Magnetizing inductor $L_m = 0.6\text{H}$
Utility grid	Line-to-Line RMS voltage $U = 380\text{V}$
	Line-frequency $f_0 = 50\text{Hz}$
	Internal inductor $L_g = 2.3\text{mH}$
Unbalanced real and reactive load	Phase A: $R_{ua} = 60\Omega$
	Phase B: $R_{ub} = 20\Omega$, $C_u = 120\mu\text{F}$
	Phase C: $R_{uc} = 25\Omega$
Nonlinear load	Resistor loaded by the diode rectifier $R_r = 55\Omega$

(a)
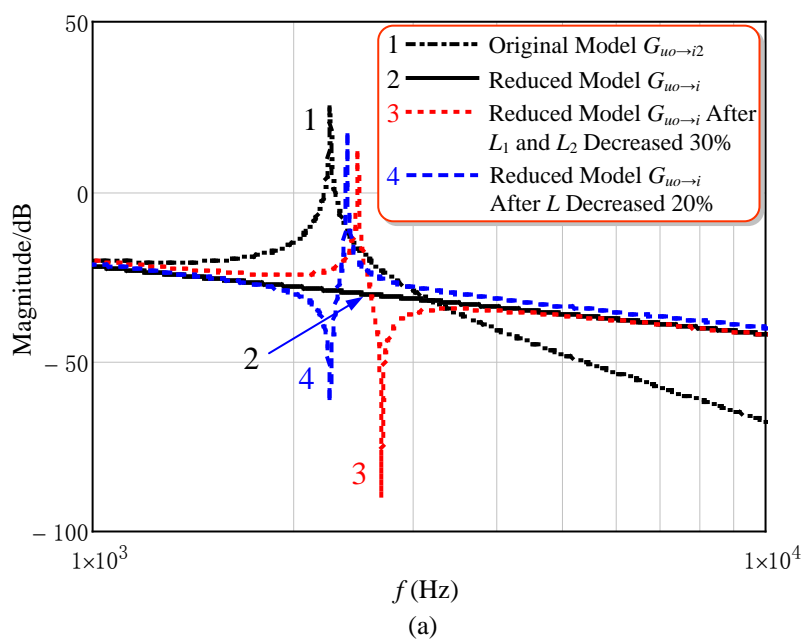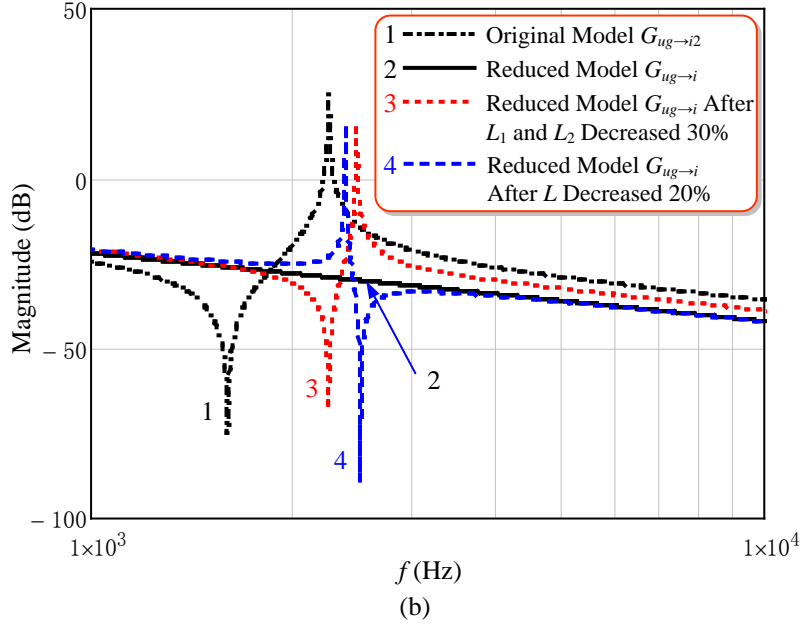
Fig. 3. Bode diagrams of the MFDGU with WACF control. (a) Bode diagram of the plant model $G_{uo \to i}$ and (b) bode diagram of the disturbance model $G_{ug \to i}$.

Fig. 2(b) shows the simplified block diagram that can be achieved by using the reduced-order model that can be used to design the PI controller. The proportional and integral gains of the PI controller can be designed according to [33].

From (14), due to the utility disturbance, actual output current of the MFDGU may deviate from its reference value. However, as shown in Fig. 2(c), a feed-forward controller $W_f(s)$ can be employed to attenuate the disturbance and enhance the dynamic performance. As shown in Fig. 2(c), the feed-forward controller is able to cancel the u_g disturbance from the virtual output current i viewpoint [36]. Therefore, the feed-forward controller should satisfy W_f $(s)K_{pwm}G_{uo \to i}(s)U_g(s) + G_{ug \to i}(s) U_g(s) = 0$. So that, the feed-forward controller can be expressed as

$$W_f(s) = -\frac{G_{u_g \to i}(s)}{K_{pwm}G_{u_o \to i}(s)} = \frac{1}{K_{pwm}} \tag{18}$$

2.2 Current reference generator algorithm

13

To enable the functionalities such as power tracking and power quality enhancement, an effective algorithm that generates the current reference should be designed for the MFDGU. As shown in Fig. 4, the current reference consists of two parts. One is used to track the power generation of the MFDGU following the given active and reactive power. The other focuses on the compensation of power quality issues at the PCC. To avoid complicated computations, the Clarke transformation is implemented:

$$\boldsymbol{T}_{abc/\alpha\beta} = \sqrt{\frac{2}{3}} \begin{bmatrix} 1 & -1/2 & -1/2 \\ 0 & \sqrt{3}/2 & -\sqrt{3}/2 \end{bmatrix} \tag{19}$$

where its inverse transformation can be written as $\boldsymbol{T}_{\alpha\beta/abc} = \boldsymbol{T}_{abc/\alpha\beta}^{T}$. If the commanded active and reactive power generation of the MFDGU is P and Q, the current references $i_{ref\alpha}$ and $i_{ref\beta}$ for the power tracking satisfy

$$\begin{cases} P = u_{g\alpha}i_{ref\alpha} + u_{g\beta}i_{ref\beta} \\ Q = u_{g\beta}i_{ref\alpha} - u_{g\alpha}i_{ref\beta} \end{cases} \tag{20}$$

where $u_{g\alpha}$ and $u_{g\beta}$ are the utility voltage in $\alpha\beta$ frame. According to (20), the power generation tracking part of the current references in $\alpha\beta$ frame can be expressed as

$$\begin{cases} i_{ref\alpha} = (u_{g\alpha}P + u_{g\beta}Q)\big/(u_{g\alpha}^2 + u_{g\beta}^2) \\ i_{ref\beta} = (u_{g\beta}P - u_{g\alpha}Q)\big/(u_{g\alpha}^2 + u_{g\beta}^2) \end{cases} \tag{21}$$

Therefore, the current reference for the power generation in natural *abc* frame i_{gabc} can be obtained by using the inverse Clarke transformation.

Ref [37] documented several methods to obtain the reactive, harmonic, and unbalanced current components for power quality enhancement. In this paper, FBD theory is used to generate the compensation part of the current reference, due to its simplicity, effectiveness and reliability features, which can be easily implemented on a DSP control board [38]. The basic idea of FBD theory is to consider the actual circuit model of the load as a set of equivalent conductances and susceptances in parallel. As shown in Fig. 4, for the MFDGU

application, if the instantaneous active power of the local non-linear and unbalanced loads is denoted as p, the totally equivalent conductance can be expressed as

$$G = p\big/(u_{g\alpha}^2 + u_{g\beta}^2) = (u_{g\alpha}i_{L\alpha} + u_{g\beta}i_{L\beta})\big/(u_{g\alpha}^2 + u_{g\beta}^2) \tag{22}$$

where $i_{L\alpha}$ and $i_{L\beta}$ are measured load current i_{Labc} in $\alpha\beta$ frame. After G is filtered by a low pass filter (LPF), the remainder G_1 corresponds to the positive-sequence fundamental active power and current of the equivalent downstream load of the MFDGU. Therefore, the positive-sequence fundamental active components of load current in $\alpha\beta$ frame can be written as

$$\begin{cases} i_{L1\alpha} = G_1 u_{g\alpha} \\ i_{L1\beta} = G_1 u_{g\beta} \end{cases} \tag{23}$$

Similarly, the positive-sequence fundamental active components in the *abc* frame i_{L1abc} can be obtained according to the inverse Clarke transformation. Then, the total load current i_{Labc} minus i_{L1abc} is the command harmonic component i_{habc} for power quality enhancement. The block diagram for current reference generation is illustrated in Fig. 4. In addition, transformation T, in Fig. 4, corresponds to (21), which generates the current reference for power generation tracking. The power tracking part i_{gabc} and the power quality enhancement part i_{habc} constitute the current reference i_{refabc} as described.
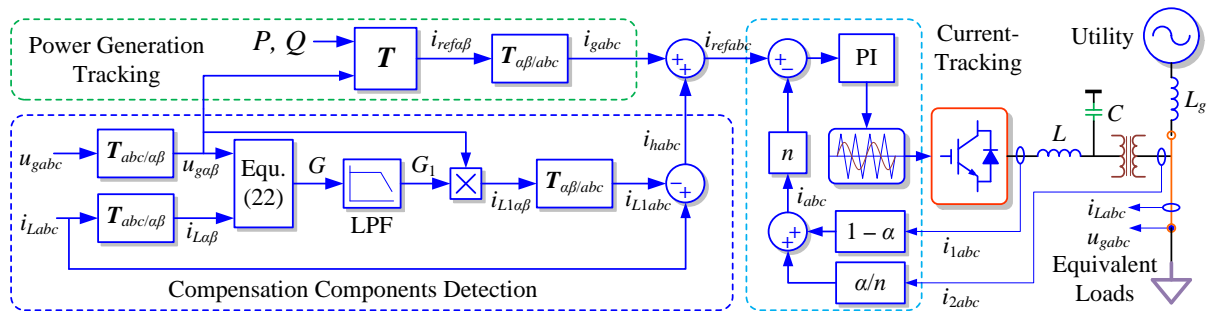

**Fig. 4. Schematic diagram of MFDGU control.**

3 Experimental results

A 15kVA prototype has been built and tested to validate the power quality improvement

performance of the MFDGU. Digital Signal Processor (DSP) TMS320F2812 is employed to realize the proposed control strategy, in which the switching frequency of the insulated gate bipolar transistors (IGBTs) is set at 10 kHz. A digital oscilloscope is used to record the waveforms. All the parameters of the prototype in Fig. 1(b) are listed in Tab. 1. The DC voltage of the MFDGU is chosen as 400V, which can be directly connected to the DC distribution network or dc-link of a DC micro-grid [39]. Besides, a step-up isolation transformer is also employed to reduce the voltage stress of IGBTs and provide galvanic isolation. Due to the low DC voltage, fewer series of PV arrays or battery units can be connected to utility through the MFDGU, compared to the traditional grid-tied inverter with high DC voltage. To suppress switching ripples, an LC filter with $L = 1\text{mH}$ and $C = 10\mu\text{F}$ is included in the MFDGU, and its cut-off frequency is 1.59kHz, which is much lower than the switching frequency (10kHz). Note that the core material type of the inductor is silicon-steel. The rated current of the inductor is 50A, and the bulk of the inductor is large measuring 220mm×150mm ×240mm.

3.1 Power generation tracking of the MFDGU

In such condition, the breakers of local loads, S_1 and S_2, are opened in Fig. 1(a). Fig. 5 demonstrates the dynamic responses of the MFDGU when its reference active power steps up from 10kW to 15kW. Note that the controller is fast enough and able to track the reference active power or reference current.
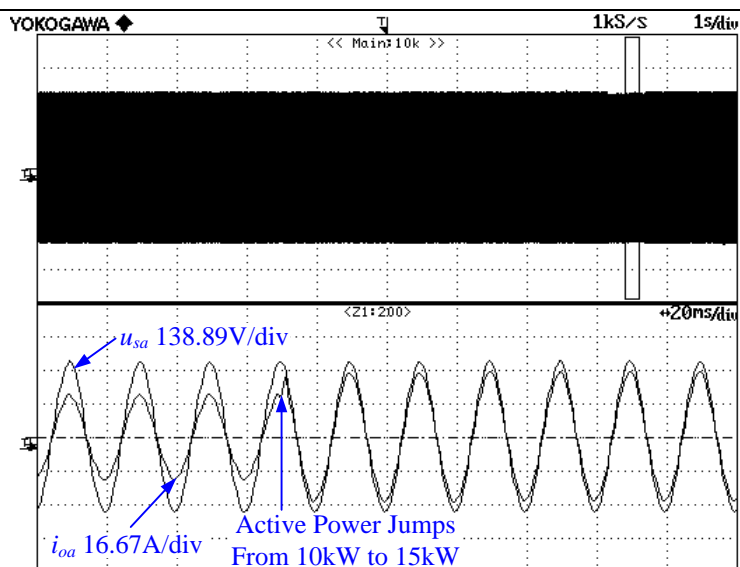
(a)
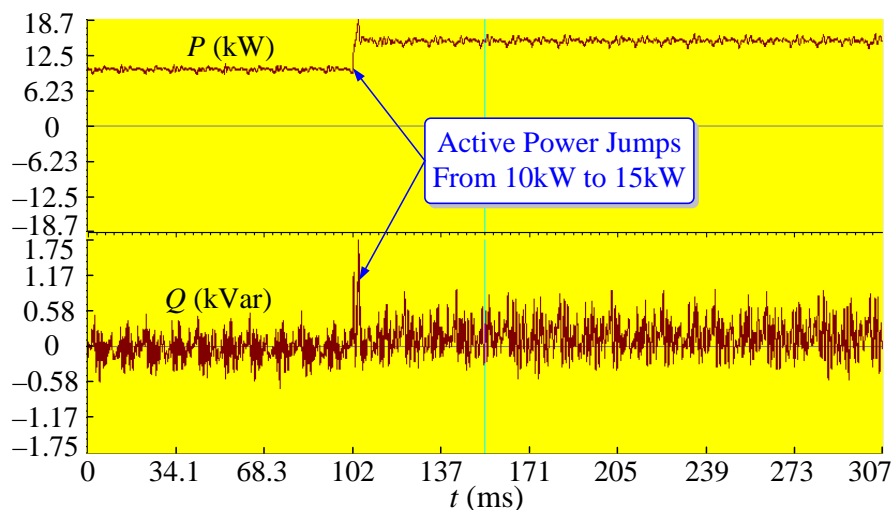
(b)

Fig. 5. Experimental results of the MFDGU when the reference active power steps. (a) Output current and the terminal voltage of the MFDGU, and (b) output power of the MFDGU.
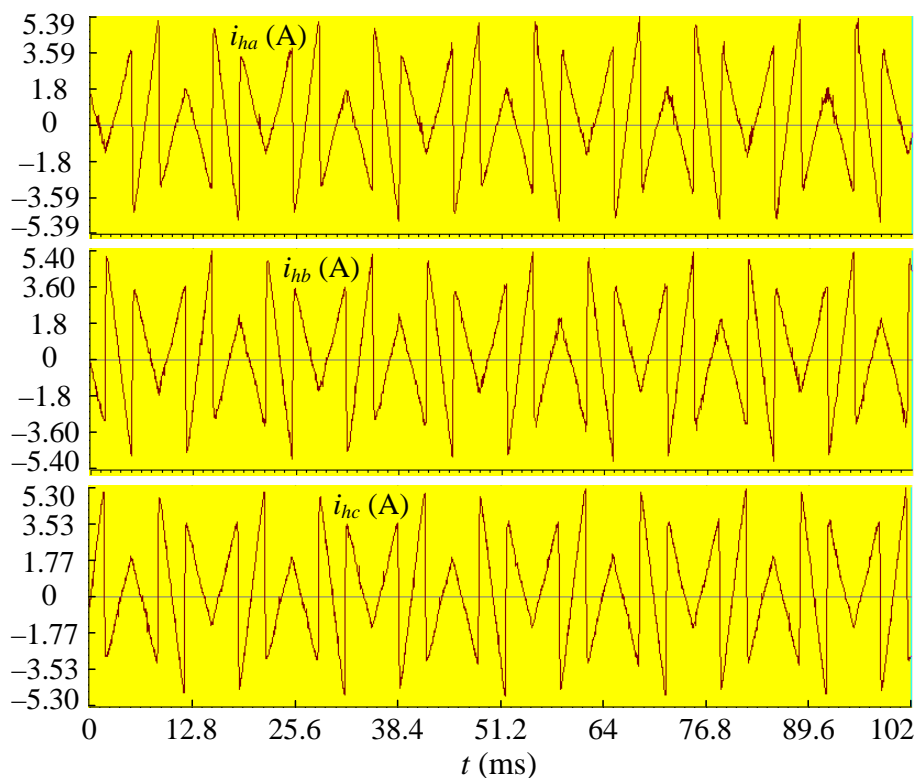
3.2 Compensation of unbalanced and reactive current

To verify the performance of the MFDGU on unbalanced and reactive current compensation, the line connected to the non-linear load is disconnected. In other words, breaker S_2 is open and breakers S_1 and S_g are closed in Fig. 1(a). Besides, the power generation tracking references for the MFDGU is set as $P = 10\text{kW}$ and $Q = 0\text{Var}$.

17

Figs. 6(a) and Fig. 6(b) indicate the equivalent conductance of load and its value filtered by the LPF. It can be found that the FBD theory is effective to detect the fundamental and compensation components of the local load current. The waveforms of grid-connected current and instantaneous power on the utility-side of the MFDGU are shown in Fig. 7. Before the MFDGU activates the power quality enhancement function, instantaneous active and reactive waveforms oscillate at twice line-frequency due to the unbalanced load [40]. It is also seen that there is a negative dc component in the instantaneous reactive power curve due to the capacitive load connected in phase *b*. After MFDGU starts to enhance power quality, the currents are symmetrical from the viewpoint of the utility. Furthermore, the power fluctuation is well suppressed and the instantaneous reactive power is fixed to zero. As a result, unity power factor is achieved at the PCC. It should be noted that the output current and the instantaneous power can track their references fast. In conclusion, the proposed MFDGU not only effectively compensates the unbalanced and reactive currents of local loads, but also greatly enhances the power quality at the PCC with good dynamic response.


(a)

(b)

(c)
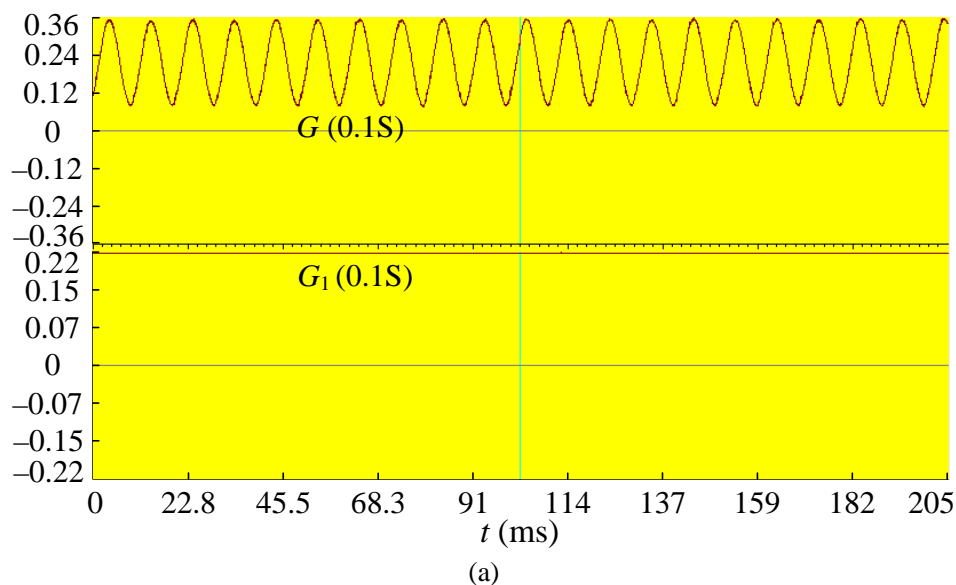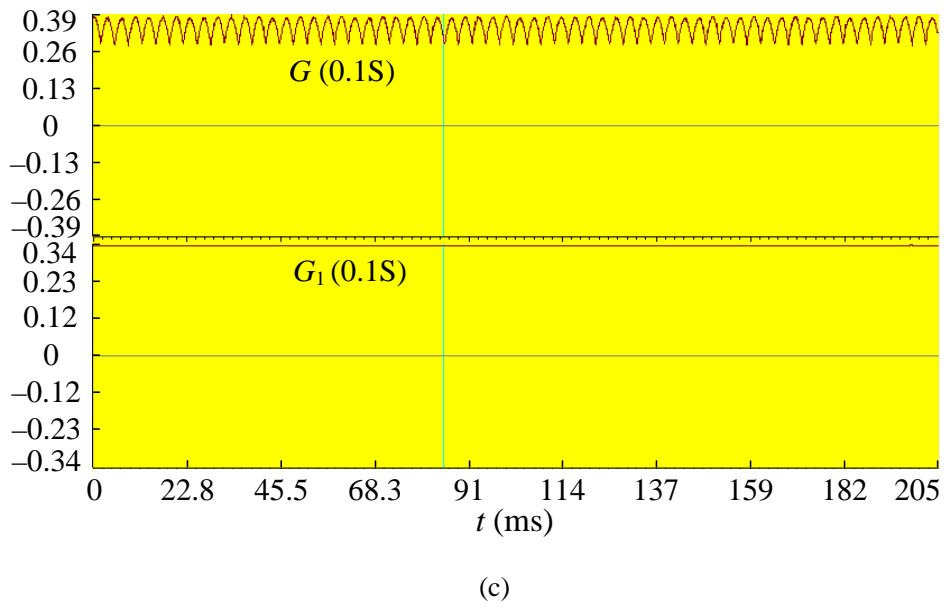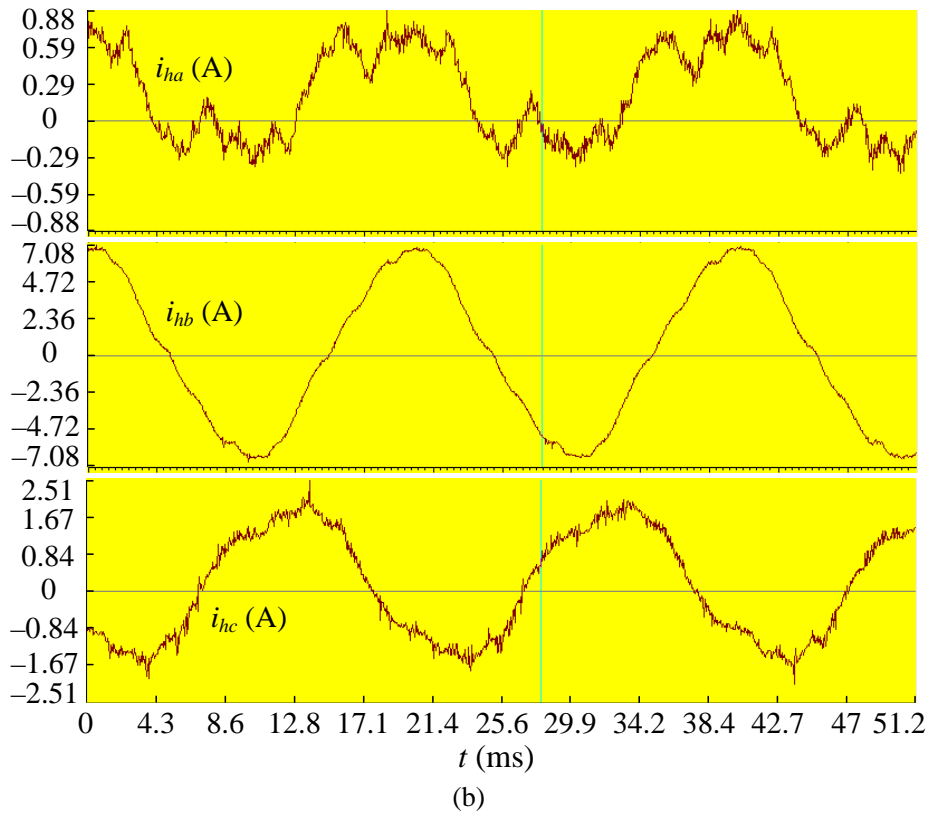
(d)

Fig. 6. Experimental results of the measured equivalent conductance of loads based on FBD theory.

(a) Conductance in the unbalanced and reactive load condition, (b) instantaneous compensation current in the unbalanced and reactive load condition, (c) conductance in non-linear load condition, (d) instantaneous compensation current in non-linear load condition.
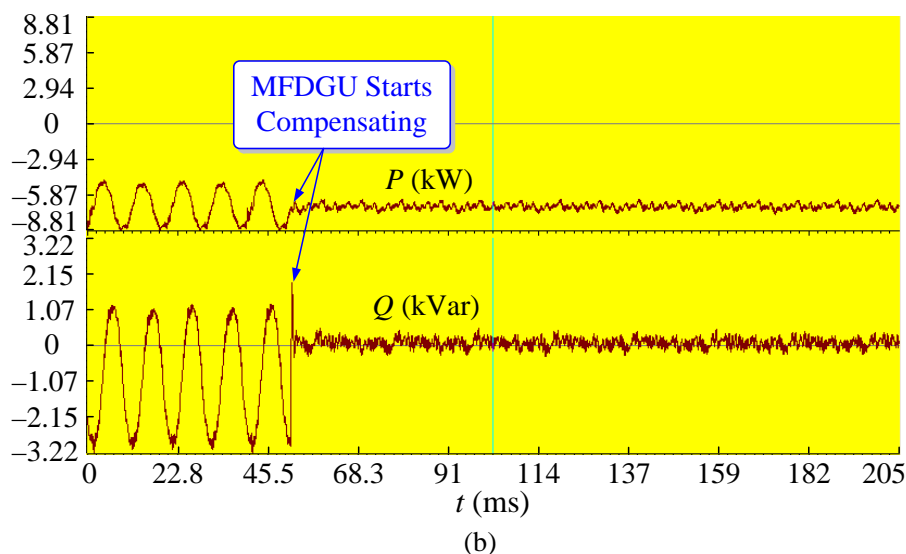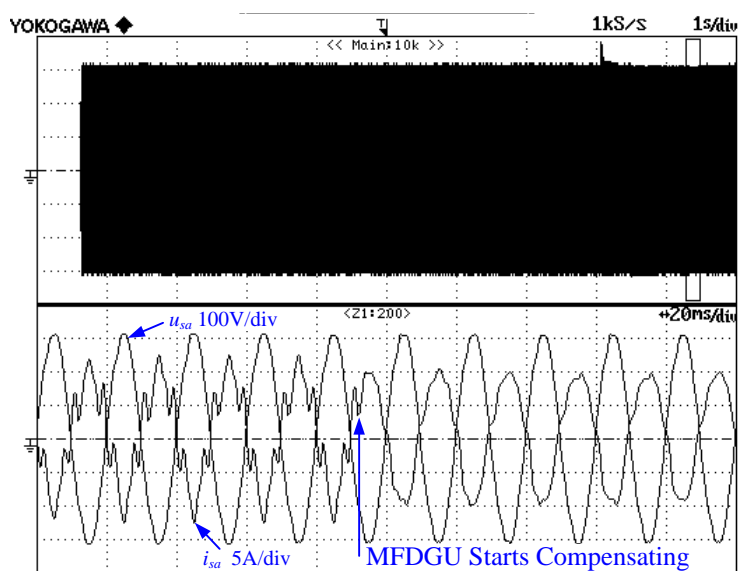

(a)

(b)
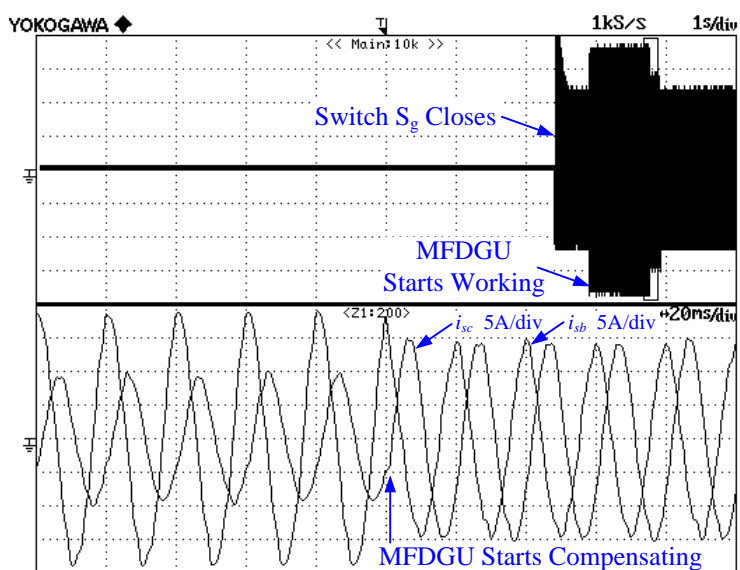
Fig. 7. Experimental results of the MFDGU to compensate unbalanced and reactive current at PCC. (a) Grid-connected current at the utility-side of the MFDGU and (b) instantaneous power at the utility-side of the MFDGU.

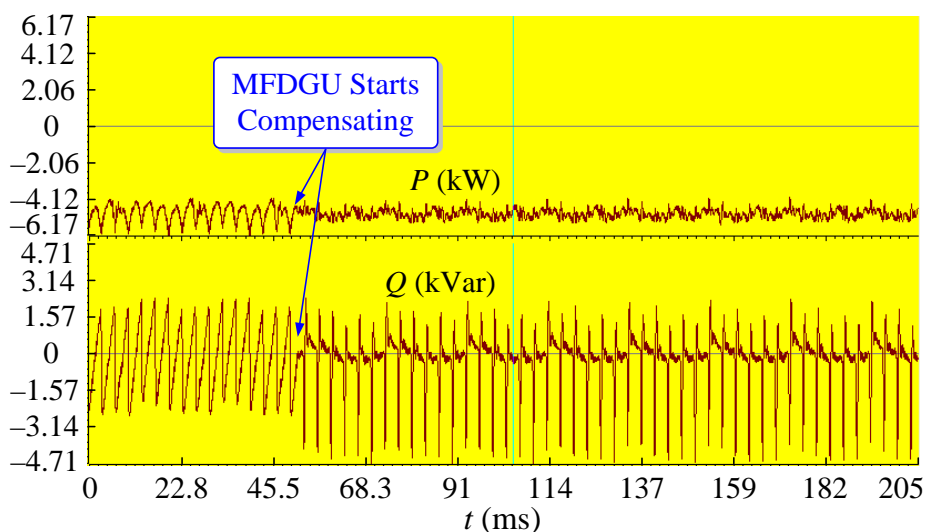### 3.3 Compensation of harmonic current

To verify the harmonic compensation capability of the MFDGU, the non-linear load is activated, i.e., circuit breaker S_1 is opened, while circuit breakers S_2 and S_g are closed in Fig. 1(a). The non-linear load is a diode rectifier loaded by a resistance R_r on the DC side. Besides, the power generation tracking command of the MFDGU is $P = 10kW$ and $Q = 0Var$.

Fig. 6(c) shows the measured equivalent conductance of non-linear load. For a diode rectifier load, the equivalent conductance fluctuates at six times of the line-frequency. Additionally, as shown in Fig. 6(c), the positive-sequence active power fundamental current component of G_1 can be accurately detected by FBD theory. Fig. 6(d) also shows the performance of the FBD-based detection algorithm. Waveforms of grid-connected current and instantaneous power on the utility-side of the MFDGU are shown in Fig. 8. Before the MFDGU starts to enhance the power quality at the PCC, it injects pure sinusoidal current into the utility. However, due to the harmonic load current of the diode rectifier, the grid-injected current at the PCC is seriously distorted. After the MFDGU activates its power quality

21

enhancement function, the distorted utility current is effectively compensated by the MFDGU, and the fluctuation of power curves caused by the distorted current is also significantly eliminated. It should be noted that, the utility voltage and current, namely u_{ga} and i_{ga}, are in anti-phase due to the defined reference directions of current in Fig. 1(a). Additionally, the instantaneous power curves fluctuate slightly after the MFDGU starts its power quality function, as shown in Fig. 8(b). According to Fig. 8(c), the total harmonic distortion (THD) of grid current i_s at the PCC is decreased from 16.12% to 6.37% after the power quality enhancement function of the MFDGU is activated. Thus, owing to the MFDGU operation, the power quality at PCC is greatly enhanced.
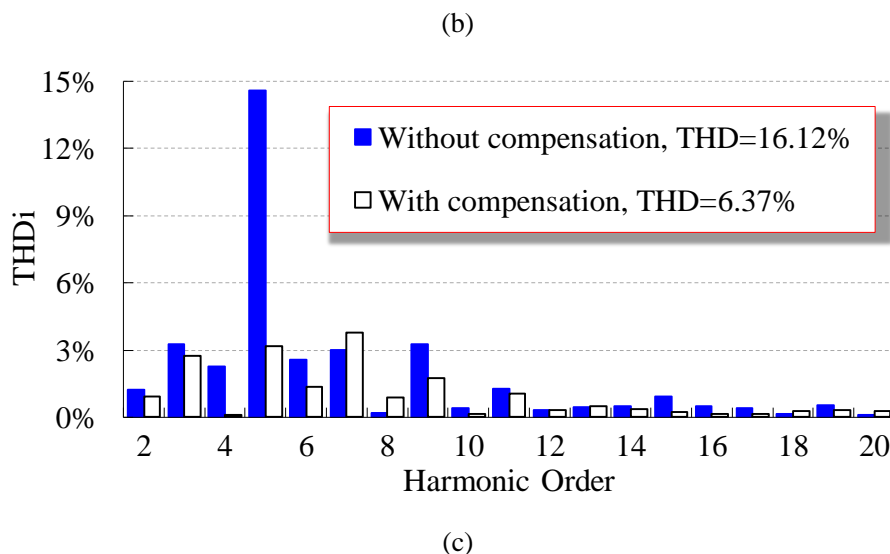

(a)

(b)

(c)

Fig. 8. Experimental results of the MFDGU to compensate harmonic current at PCC. (a) Grid-connected current at the utility-side of the MFDGU, (b) instantaneous power at the utility-side of MFDGU, and (c) harmonic distribution of the utility current i_{ga} before and after MFDGU compensates power quality issues.

In summary, according to the aforementioned experimental results, the proposed MFDGU topology and its control scheme are effective to integrate RESs into the utility grid and to enhance, to some extent, the power quality at the PCC. Due to its several independent features, MFDGU would have the potential to be broadly applied in DGSs to partly substitute the additional power quality conditioners.

4 Discussions

To realize the ancillary service for power quality enhancement, the MFDGU should generate reactive and harmonic current to utility. As a result, it may influence the reliability of IGBTs, even though the reliability of common grid-connected inverter is already relatively low [41]. Therefore, future work should be made to study reliability-based MFDGU applications.

For the application of MFDGU in practice, the strategic placement and coordinated control of multiple MFDGUs should be studied.

On one hand, as shown in Fig. 1(a), a special T-type structure at the grid-connection point of the MFDGU confirms that the MFDGU module can be connected at any point of a DGS in the same way as a conventional grid-connected inverter. It can be found that, no matter where the MFDGU is, downstream or on the load-side of the MFDGU can be viewed as an equivalent load, and the power quality at upstream or on the utility-side of the MFDGU can be greatly enhanced after the power quality issues of the equivalent load are compensated by the MFDGU. Therefore, the proposed scheme does not require strategic placement of MFDGU. In instead, the MFDGU can be placed at any point of a DGS like a normal grid-connected inverter.

On the other hand, how to coordinate multiple MFDGUs in a DGS should be paid adequate attention. However, this issue is out of the scope of this paper which focuses controlling and verifying a 3H-bridge-based MFDGU with the functionality of power quality enhancement. A coordinated control of multiple MFDGUs via conductance and susceptance limitation can be found in [31].

5 Conclusions

This paper has proposed and experimentally verified an MFDGU and its control strategy for DGS applications. The function of power generation tracking of conventional grid-connected converters and the function of the power quality enhancement of power quality conditioners are combined in the proposed MFDGU. To overcome the complexity of its full-order mathematical model, a reduced-order model is studied by using the WACF approach. Detailed discussions on the stability and robustness of the model in terms of mathematics and physics are also provided. To achieve the intended functions of the MFDGU, an effective algorithm to generate its current reference is also proposed. Experimental results have verified the power quality enhancement feature of the 3H-bridge-based MFDGU.

6 Acknowledgments

References

[1] Xin, T., Tsang, K.M., Chan, W.L.: 'A power quality compensator with DG interface capability using repetitive control', *IEEE Trans. on Energy Convers.*, 2012, **27**, (2), pp. 213-219

[2] Zeng, Z., Yang, H., Zhao, R.: 'Study on small signal stability of microgrids: A review and a new approach', *Renew. Sust. Energy Rev.*, 2011, **15**, (9), pp. 4818-4828

[3] Nutkani, I.U., Loh, P.C., Blaabjerg, F.: 'Power flow control of intertied ac microgrids', *IET Power Electron.*, 2013, **6**, (7), pp. 1329–1338

[4] Rocabert, J., Luna, A., Blaabjerg, F., Rodri, X., Guez, P.: 'Control of power converters in AC microgrids', *IEEE Trans. on Power Electron.*, 2012, **27**, (11), pp. 4734-4749

[5] Blaabjerg, F., Chen, Z., Kjaer, S.B.: 'Power electronics as efficient interface in dispersed power generation systems', *IEEE Trans. on Power Electron.*, 2004, **19**, (5), pp. 1184-1194

[6] Chakraborty, S., Kramer, B., Kroposki, B.: 'A review of power electronics interfaces for distributed energy systems towards achieving low-cost modular design,' *Renew. Sust. Energy Rev.*, 2009, **13**, (9), pp. 2323-2335

[7]   Xiao, H., Liu, X., Lan, K.: 'Optimised full-bridge transformerless photovoltaic grid-connected inverter with low conduction loss and low leakage current', *IET Power Electron.*, 2014, **7**, (4), pp. 1008–1015

[8]   Singh, B., Shahani, D.T., Verma, A.K.: 'Neural network controlled grid interfaced solar photovoltaic power generation', *IET Power Electron.*, 2014, **7**, (3), pp. 614–626

[9]   Enslin J.H.R., Heskes, P.J.M.: 'Harmonic interaction between a large number of distributed power inverters and the distribution network', *IEEE Trans. on Power Electron.*, 2004, **19**, (6), pp. 1586-1593

[10]   Zeng, Z., Zhao, R., Yang, H., Cheng, C.: 'Topologies and control strategies of multi-functional grid-connected inverters for power quality enhancement: A comprehensive review', *Renew. Sust. Energy Rev.*, 2013, **24**, pp. 223-270

[11]   Hu, J.B., Nian, H., Xu, H.L., He, Y.K.: 'Dynamic modeling and improved control of DFIG under distorted grid voltage conditions', *IEEE Trans. on Energy Convers.*, 2011, **26**, (1), pp. 163-175

[12]   Roscoe, A.J., Finney, S.J., Burt, G.M.: 'Tradeoffs between ac power quality and dc bus ripple for 3-phase 3-wire inverter-connected devices within microgrids', *IEEE Trans. on Power Electron.*, 2011, **26**, (3), pp. 674-688

[13]   Hornik, T., Zhong, Q.C.: 'A current-control strategy for voltage-source inverters in microgrids based on H∞ and repetitive control', *IEEE Trans. on Power Electron.*, 2011, **26**, (3), pp. 943-952

[14]   Ghosh, A., Ledwich, G.: 'Compensation of distribution system voltage using DVR', *IEEE Trans. on Power Del.*, 2002, **17**, (4), pp. 1030-1036

[15] Xu, Y., Tolbert, L.M., Kueck, J.D., Rizy, D.T.: 'Voltage and current unbalance compensation using a static var compensator', *IET Power Electron.*, 2010, **3**, (6), pp. 977-988

[16] Xie, H.L., Angquist, L., Nee, H.P.: 'Investigation of StatComs with capacitive energy storage for reduction of voltage phase jumps in weak networks', *IEEE Trans. on Power Syst.*, 2009, **24**, (1), pp. 217-225

[17] Leon, A.E., Amodeo, S.J., Solsona, J.A., Valla, M.I.: 'Non-linear optimal controller for unified power quality conditioners', *IET Power Electron.*, 2011, **4**, (4), pp. 435-446

[18] Wu, T.F., Hien, H.S., Hsieh, H.M., Shen, C.L.: 'PV power injection and active power filtering with amplitude-clamping and amplitude-scaling algorithms', *IEEE Trans. on Ind. Appl.*, 2007, **43**, (3), pp. 731-741

[19] Singh, M., Khadkikar, V., Chandra, A.: 'Grid synchronization with harmonics and reactive power compensation capability of a permanent magnet synchronous generator-based variable speed wind energy conversion system', *IET Power Electron.*, 2011, **4**, (1), pp. 122-130

[20] Sawant, R.R., Chandorkar, M.C.: 'Methods for multi-functional converter control in three-phase four-wire systems', *IET Power Electron.*, 2009, **2**, (1), pp. 52-66

[21] Majumder, R., Ghosh, A., Ledwich, G., Zare, F.: 'Load sharing and power quality enhanced operation of a distributed microgrid', *IET Renewable Power Generation*, 2009, **3**, (2), pp. 109-119

[22] Prodanovic, M., De Brabandere, K., Van Den Keybus, J., Green, T., Driesen, J.: 'Harmonic and reactive power compensation as ancillary services in inverter-based

distributed generation', *IET Generation, Transmission and Distribution*, 2007, **1**, (3), pp. 432-438, 2007

[23]   Todeschini, G., Emanuel, A.E.: 'Wind energy conversion systems as active filters: Design and comparison of three control methods', *IET Renewable Power Generation*, 2010, **4**, (4), pp. 341-353.

[24]   Guerrero, J.M., Vasquez, J.C., Matas, J., Vicuna, L.G., Castilla, M.: 'Hierarchical control of droop-controlled AC and DC microgrids - A general approach toward standardization', *IEEE Trans. on Ind. Electron.*, 2011, **58**, (1), pp. 158-172

[25]   Wang, F., Duarte, J.L., Hendrix, M.A.M.: 'Grid-interfacing converter systems with enhanced voltage quality for microgrid application: Concept and implementation', *IEEE Trans. on Power Electron.*, 2011, **26**, (12), pp. 3501-3513

[26]   Prodanovic, M., Green, T.C.: 'High-quality power generation through distributed control of a power park microgrid', *IEEE Trans. on Ind. Electron.*, 2006, **53**, (5), pp. 1471-1482

[27]   Bojoi, R.I., Limongi, L.R., Roiu, D., Tenconi, A.: 'Enhanced power quality control strategy for single-phase inverters in distributed generation systems', *IEEE Trans. on Power Electron.*, 2011, **26**, (3), pp. 798-806

[28]   Li, Y.W., Kao, C.N.: 'An accurate power control strategy for power-electronics-interfaced distributed generation units operating in a low-voltage multibus microgrid', *IEEE Trans. on Power Electron.*, 2009, **24**, (12), pp. 2977-2988

[29]   Li, Y.W., Vilathgamuwa, D.M., Poh, C.L.: 'Microgrid power quality enhancement using a three-phase four-wire grid-interfacing compensator', *IEEE Trans. on Ind. Appl.*, 2005, **41**, (6), pp. 1707-1719

[30]   Majumder, R., Ghosh, A., Ledwich, G., Zare, F.: 'Load sharing and power quality enhanced operation of a distributed microgrid', *IET Renew. Power Gener.*, 2009, **3**, (2), pp. 109-119

[31]   Zeng, Z., Zhao, R., Yang, H.: 'Coordinated control of multi-functional grid-tied inverters using conductance and susceptance limitation', *IET Power Electron.*, 2014, **7**, (x), pp. xx-xx

[32]   Guerrero, J.M., Matas, J., Vicuna, L.G., Castilla, M., Miret, J.: 'Wireless-control strategy for parallel operation of distributed-generation inverters', *IEEE Trans. on Ind. Electron.*, 2006, **53**, (5), pp. 1461-1470

[33]   Dannehl, J., Wessels, C., Fuchs, F.W.: 'Limitations of voltage-oriented PI current control of grid-connected PWM rectifiers with LCL filters', *IEEE Trans. on Ind. Electron.*, 2009, **56**, (2), pp. 380-388

[34]   Guo, X.Q., Wu, W.Y., Gu, H.R.: 'Modeling and simulation of direct output current control for LCL-interfaced grid-connected inverters with parallel passive damping', *Simulation Modelling Practice and Theory*, 2010, **18**, pp. 946-956

[35]   Shen, G., Xu, D., Cao, L., Zhu, X.: 'An improved control strategy for grid-connected voltage source inverters with an LCL filter', *IEEE Trans. on Power Electron.*, 2008, **23**, (4), pp. 1899-1906

[36] Wang, X.H., Ruan, X.B., Liu, S.W., Tse, C.K.: 'Full feedforward of grid voltage for grid-connected inverter with LCL filter to suppress current distortion due to grid voltage harmonics,' *IEEE Trans. on Power Electron.*, 2010, **25**, (12), pp. 3119-3127

[37] Asiminoael, L., Blaabjerg, F., Hansen, S.: 'Detection is key - Harmonic detection methods for active power filter applications', *IEEE Ind. Appl. Mag.*, 2007, **13**, (4), pp. 22-33

[38] Akagi, H., Watanabe, E.H., Aredes, M.: 'Instantaneous power theory and applications to power conditioning', (John Wiley & Sons, Inc., 2007)

[39] Loh, P.C., Li, D., Chai, Y.K., Blaabjerg, F.: 'Autonomous operation of ac–dc microgrids with minimised interlinking energy flow', *IET Power Electron.*, 2013, **6**, (8), pp. 1650-1657

[40] Hu, J.B. , He, Y.K.: 'Modeling and control of grid-connected voltage-sourced converters under generalized unbalanced operation conditions', *IEEE Trans. on Energy Convers.*, 2008, **23**, (3), pp. 903-913

[41] Yang, S., Bryant, A.T., Mawby, P.A., Xiang, D., Ran, L., Tavner, P.: 'An industry-based survey of reliability in power electronic converters', *IEEE Trans. Ind. Appl.*, 2011, **47**, (3), pp. 1441–1451